

AutoPot: Automated and massively parallelized construction of Machine-Learning Potentials

M. Hodapp¹ and G. Anciaux²

¹Christian Doppler Laboratory for Digital material design guidelines for mitigation of alloy embrittlement, Materials Center Leoben Forschung GmbH (MCL), Leoben (AT)

²Ecole Polytechnique Federale de Lausanne (EPFL), Lausanne (CH)

January 6, 2026

Abstract

Machine-learning potentials (MLIPs) have been a breakthrough for computational physics in bringing the accuracy of quantum mechanics to atomistic modeling. To achieve near-quantum accuracy, it is necessary that neighborhoods contained in the training set are rather close to the ones encountered during a simulation. Yet, constructing a single training set that works well for all applications is, and likely will remain, infeasible, so, one strategy is to supplement training protocols for MLIPs with additional learning methods, such as active learning, or fine-tuning. This strategy, however, yields very complex training protocols that are difficult to implement efficiently, and cumbersome to interpret, analyze, and reproduce.

To address the above difficulties, we propose AutoPot, a software for automating the construction and archiving of MLIPs. AutoPot is based on BlackDynamite, a software operating parametric tasks, e.g., running simulations, or single-point ab initio calculations, in a highly-parallelized fashion, and Motoko, an event-based workflow manager for orchestrating interactions between the tasks. The initial version of AutoPot supports selection of training configurations from large training candidate sets, and on-the-fly selection from molecular dynamics simulations, using Moment Tensor Potentials as implemented in MLIP-2, and single-point calculations of the selected training configurations using VASP. Another strength of AutoPot is its flexibility: BlackDynamite tasks and orchestrators are Python functions to which own existing code can be easily added and manipulated without writing complex parsers. Therefore, it will be straightforward to add other MLIP and ab initio codes, and manipulate the Motoko orchestrators to implement other training protocols.

1 Introduction

Machine-learning interatomic potentials (MLIPs) [1, 2, 3, 4, 5, 6, 7, 8, 9, 10, 11, 12, 13] have revolutionized computational materials science by overcoming the two persisting limitations of empirical interatomic potentials:

- MLIPs are able to predict mechanisms that influence defect motion, stability of crystal structures, etc., of a hypothetical large-scale quantum-mechanical simulation, enabling quantum-accurate multiscale simulations up to the continuum level (e.g., [14]).
- MLIPs are able to predict the influence of variations of the chemistry on material properties that, e.g., enables exploring trends in the composition of complex concentrated alloys (e.g., [15, 16, 17]).

Despite these success stories, achieving predictive accuracy requires a carefully designed training set containing atomic neighborhoods that are not too far from those encountered during a simulation of the material behavior, which is a time-consuming task. Random sampling of training configuration before running a simulation is often not accurate enough, or requires a lot of training configurations [18, 19, 20, 21, 22, 23], so, protocols for constructing MLIP training sets are complemented with advanced sampling algorithms, e.g., active learning [24] from simulations that resemble the underlying problem of interest [25, 26, 27, 28, 29]. Another related problem is fine-tuning a MLIP that has been pre-trained on a (generally very large) dataset using additional problem-specific configurations (e.g., [30]).

Such algorithms already have a certain complexity in that they require communication between several software codes, i.e., the code that implements the potential, the code that runs the ab initio calculations, and a code that

maxludwig.hodapp@mcl.at
guillaume.anciaux@epfl.ch

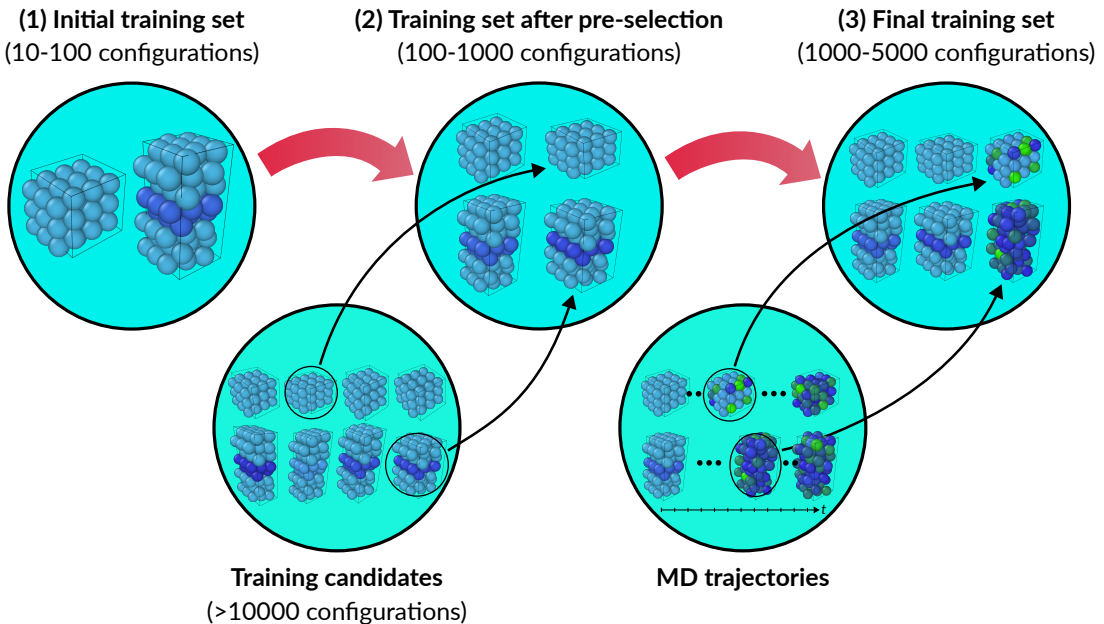


Figure 1: Schematic of the active learning workflow implemented in AutoPot: (1) Starting from an initial training set, (2) AutoPot adds the most uncertain configurations from a large set of training candidates, (3) followed by a selection of training configurations from MD trajectories

runs the simulation from which configurations are sampled from. Developing and implementing such algorithms becomes more and more difficult with an increasing complexity of MLIPs. For example, Kotykhov et al. [31] proposed an active learning algorithm that trains a magnetic MLIP on spin-constrained Density Functional Theory (DFT) calculations during MD simulations. Capturing realistic atomic trajectories of magnetic materials requires a hybrid approach combining molecular dynamics and Monte Carlo simulations, so, potentially two simulation codes from which configurations are sampled from. Therefore, making such algorithms constructing MLIPs more flexible, reliable, and reproducible requires, streamlining training protocols.

At the center of active learning stands the creation and storage of configuration datasets, a *sine qua non* condition to incrementally train MLIPs. New configurations will be dynamically selected, created, and interleaved, with training phases. For reproducibility reasons, it is crucial to keep the link existing between intermediate results down to the final potential. Therefore, the storage of configurations, training sets, algorithms inputs and outputs (MD, DFT, training), need to be saved and organized to enable a machine learning model following open science and FAIR [32] principles.

With similar goals, there exist several workflow management services, for general purposes [33, 34, 35, 36, 37], or for specific material science applications [38, 39, 40, 41, 42, 43, 44, 45]. All these approaches allow to easily manipulate training sets, especially when they are in classical forms (e.g. tables and images). However, these services and tools are not easily tunable for less standard fields of research. For instance, these automation tools struggle to handle rare scenarios arising during simulations (e.g. unexpected configurations needing live re-training), but also to adapt to user-level permissions and constraints appearing when using HPC facilities.

Furthermore, the above tools have generally a destructive approach regarding intermediate results, which may prevent full reproducibility. Concretely, a workflow manager such as *Flyte* [37] will use anonymous runs and preserve only minimal (meta-)data in output databases. This cloud-based relation with data storage is frugal, but requires the workflow to be mature to guaranty that all necessary information is kept. When developing a workflow, or when someone wants to re-use a previous execution, or explore new orchestration directions, it becomes a limitation. Another consequence of such a data-flow, is that past tasks/jobs cannot easily be queried and/or be used by the global orchestrator to construct and alter workflow and orchestration decisions.

In the current work, we will present a workflow allowing MLIPs, to be obtained through active learning, where tasks are 1) producing configurations, 2) selecting configurations based on the MLIP’s uncertainty, 3) single point evaluation of energy, forces, and stresses, and 4) training the potential, within complex iterative algorithms. To this end, we propose a novel workflow orchestrator, *Motoko* [46] that keeps every information produced by such tasks, order metadata in object-database, while providing an asynchronous python description of the global orchestration. *AutoPot* is then presented as a fully functional workflow allowing to obtain Moment Tensor Potentials [4], a class of MLIPs, by active learning based on the D-optimality criterion [24]. All details of the orchestration are accessible within an open-source repository [47].

2 Active learning for Moment Tensor Potentials

Before outlining the methodology, we establish the following notation. Consider a periodic configuration $\{\underline{r}_i\} = \{\underline{r}_i\}_{i=1}^N$ of N atoms, representing the system at a given step during an atomistic simulation. The neighborhood of the i -th atom is defined as the set $\mathcal{N} = \{\underline{r}_{ij}, z^i, \{z^j\}\}$ of all relative atomic positions $\underline{r}_{ij} = \underline{r}_j - \underline{r}_i$ between the atom located at \underline{r}_i and atoms \underline{r}_j located within a cut-off radius of a few lattice spacings from atom i , and the species of atom i , z_i , and its neighbors $\{z_j\}$. We assume that the total energy Π of $\{\underline{r}_i\}$ can be decomposed into per-atom energy contributions $\mathcal{E}(\mathcal{N})$, so that

$$\Pi(\{\underline{r}_i\}) = \sum_{\mathcal{N} \in \{\underline{r}_i\}} \mathcal{E}(\mathcal{N}). \quad (1)$$

2.1 Moment Tensor Potentials

The per-atom energies \mathcal{E} of Moment Tensor Potentials (MTPs) [4, 48] are expressed as a linear combination of basis functions B_α

$$\mathcal{E}(\mathcal{N}) = \sum_{\alpha} \xi_{\alpha} B_{\alpha}(\mathcal{N}), \quad (2)$$

with learnable coefficients ξ_{α} . The basis functions are constructed from scalar contractions of the moment tensors

$$M_{\mu, \nu}(\mathcal{N}) = \sum_{\underline{r}_{ij} \in \mathcal{N}} \sum_n c_{\mu n}(z_i, z_j) f_n(|\underline{r}_{ij}|) \underbrace{(\underline{r}_{ij} \otimes \cdots \otimes \underline{r}_{ij})}_{\nu \text{ times}}, \quad (3)$$

where the $c_{\mu n}$'s are free (nonlinear) parameters, and the f_n 's are Chebyshev radial basis functions smoothly vanishing at the potential cut-off. In equation (3), the indices μ and ν represent the moment tensor level given by $\text{lev } M_{\mu, \nu} = 2 + 4\mu + \nu$. An MTP with a level lev_{MTP} is constructed from all basis functions obtained by all scalar contractions of the $M_{\mu, \nu}$'s satisfying $\text{lev}_{\text{MTP}} \geq \sum_{i=0}^{N_{\text{m}}} \text{lev } M_{\mu_i, \nu_i}$, with N_{m} being the number of moment tensors involved in the contraction; for example, a level-16 MTP contains 92 basis functions.

The parameters ξ_{α} and $c_{\mu n}$ are obtained from a minimization of the loss function

$$\mathcal{L} = \sum_k \left(w_{\text{e}} (\Pi_k - \Pi_k^{\text{dft}})^2 + w_{\text{f}} \left(\sum_i \|\underline{f}_{k,i} - \underline{f}_{k,i}^{\text{dft}}\|^2 \right) + w_{\text{s}} \|\underline{\sigma}_k - \underline{\sigma}_k^{\text{dft}}\|^2 \right), \quad (4)$$

where Π_k , $\underline{f}_{k,i}$, and $\underline{\sigma}_k$, are the MTP energies, forces, and stresses, of a configuration k from the training set, Π_k^{dft} , $\underline{f}_{k,i}^{\text{dft}}$, and $\underline{\sigma}_k^{\text{dft}}$, are the corresponding quantities of the quantum-mechanical model on which the MTP is trained, and w_{e} , w_{f} , and w_{s} , are the weights of the three different terms.

2.2 Uncertainty quantification

Suppose now that we are given an MTP that has been trained on some number of configurations. We now want to check whether a *new* configuration $\{\underline{r}_i\}^*$, not contained in the training set, should be added to the training set so that the MTP interpolates the quantum-mechanical energy at $\{\underline{r}_i\}^*$.

The algorithm that decides whether to add this configuration to our training set is called query strategy [24]. Here, we use the well-established D-optimality criterion for MTPs [25], as implemented in MLIP-2. D-optimality estimates the MTP's uncertainty based on a scalar variable, the extrapolation grade γ (it is called extrapolation grade because, mathematically, γ has the meaning of a degree of extrapolation).

To compute γ , consider an MTP with m parameters and an active set containing m configurations. We now define the $m \times m$ Jacobian matrix

$$\underline{\underline{A}} = \begin{pmatrix} \frac{\partial \Pi(\{\underline{r}_i\}_1; \theta)}{\partial \theta_1} & \cdots & \frac{\partial \Pi(\{\underline{r}_i\}_1; \theta)}{\partial \theta_m} \\ \vdots & \ddots & \vdots \\ \frac{\partial \Pi(\{\underline{r}_i\}_m; \theta)}{\partial \theta_1} & \cdots & \frac{\partial \Pi(\{\underline{r}_i\}_m; \theta)}{\partial \theta_m} \end{pmatrix}, \quad (5)$$

where $\theta = \{\xi_{\alpha}, c_{\mu n}\}$ includes all linear and nonlinear parameters. The extrapolation grade γ is then defined as the maximum change in the determinant of $\underline{\underline{A}}$ when replacing any of the configurations from the active set with $\{\underline{r}_i\}^*$. Computing all determinants individually is unnecessary. Instead, γ can be efficiently calculated as

$$\gamma = \max_i |c_i|, \quad \text{with } \underline{\underline{\sigma}} = \left(\frac{\partial \Pi(\{\underline{r}_i\}^*; \theta)}{\partial \theta_1} \cdots \frac{\partial \Pi(\{\underline{r}_i\}^*; \theta)}{\partial \theta_m} \right)^T \underline{\underline{A}}^{-1}. \quad (6)$$

We remark that the training set typically contains many more configurations than parameters, making $\underline{\underline{A}}$ over-determined. Therefore, the m neighborhoods are selected so that linear independence of the column vectors of $\underline{\underline{A}}$ is maximized; this is done using the maxvol algorithm of Goreinov et al. [49].

To decide whether $\{\underline{r}_i\}^*$ should be added to the training set, Novikov et al. [50] defined the following classification of extrapolation grades:

| | |
|----------------------|---|
| $\gamma \leq 1$ | indicates interpolation, |
| $1 < \gamma \leq 2$ | indicates accurate extrapolation, |
| $2 < \gamma \leq 10$ | indicates still reliable extrapolation, |
| $10 < \gamma$ | indicates risky extrapolation. |

2.3 Learning protocols

Having the scalar uncertainty γ well-defined, there are now multiple ways to implement active learning algorithms in order to assemble a good training set. Below, we will describe two of them that have proven particularly useful for constructing unbiased training sets for random alloys [16, 51, 52], and are implemented in the initial version of AutoPot.

The first algorithm addresses the problem of having a large set of candidate configurations $\mathcal{T}_{\text{cand}}$ that we cannot all afford to compute with a quantum-mechanical model. To that end, Algorithm 2.1 iterates through all the configurations in the candidate set $\mathcal{T}_{\text{cand}}$, and checks whether the extrapolation grade exceeds a threshold indicating that the corresponding configuration should be added to the training set.

Algorithm 2.1: Selection

Input: MTP, training candidate set $\mathcal{T}_{\text{cand}}$, $\gamma_{\text{threshold}}$

- 1 $\mathcal{T}_{\text{selected}} \leftarrow \{\};$ // initialize set of selected configurations to be added to the training set
- 2 **for** $\{\underline{r}_i\}^* \in \mathcal{T}_{\text{cand}}$ **do**
- 3 Compute γ of $\{\underline{r}_i\}^*$ (6);
- 4 **if** $\gamma > \gamma_{\text{threshold}}$ **then**
- 5 Add $\{\underline{r}_i\}^*$ to $\mathcal{T}_{\text{selected}}$;
- 6 Update the matrix $\underline{\underline{A}}$ (5);
- 7 **end**
- 8 **end**
- 9 Run a single-point calculation on each configuration in $\mathcal{T}_{\text{selected}}$, and add them to the training set;
- 10 Re-train the MTP on the updated training set;

Output: New MTP

When making selections from large sets of training candidates, Algorithm 2.1 is typically called iteratively, with decreasing $\gamma_{\text{threshold}}$'s as input. The reasoning behind this strategy is as follows: suppose that training candidates are ordered with increasing extrapolation grade, i.e. increasing distance from the training set. Then, after adding the first candidate to $\mathcal{T}_{\text{select}}$ and updating the matrix $\underline{\underline{A}}$, the next candidate may still have an extrapolation above $\gamma_{\text{threshold}}$ and will be added to $\mathcal{T}_{\text{select}}$. In practice, however, it suffices to add the candidate with the *highest* extrapolation to $\mathcal{T}_{\text{select}}$ so that all other candidates are interpolated by the potential. This strategy therefore ensures that the chance of selecting too many similar configurations is strongly reduced, keeping the training set small without sacrificing accuracy (cf. [51]).

The second algorithm addresses the problem of a training candidate set not being representative enough to ensure a certain level of accuracy of a simulation using the MTP, or even to ensure the stability of the simulation. In such cases, we need to sample the training configurations on-the-fly while running the simulations, e.g., structural relaxation, molecular dynamics, Monte Carlo simulations, etc. Algorithm 2.2 exemplifies the main steps of such a sampling procedure.

While the above algorithms have been successfully applied to construct reliable MLIPs, it remains difficult to implement them efficiently. One of the challenges is that such algorithms cannot be run using a single software but requires at least two, the code that implements the MLIP, and the code that implements the ab initio model. In case of Algorithm 2.2, even a third code is possibly required that runs the simulation.

Another challenge is that the codes need not only communicate with each other in a sequential manner. Instead, their execution may need to follow a highly heterogeneous pattern. For example, in Algorithm 2.2, we may sample from many (possibly thousands) of simulations each triggering new single-point calculations at different points in time. In such cases, we do not want to wait until *all* simulations are finished. Instead, we want to run the single-point calculations immediately, while other simulations continue running. This requires a workflow manager that allows to place conditions on individual simulations based on which another simulation is started.

The main aim of the present work is to demonstrate that the above challenges can be addressed using a novel workflow orchestrator based on the BlackDynamite framework. We will describe the key building blocks in the following.

Algorithm 2.2: On-the-fly selection

Input: MTP, configurations $\{\underline{r}_i\}_j$ on which to run the simulations, thresholds γ_{\min} and γ_{\max}

1 $\mathcal{T}_{\text{cand}} \leftarrow \{\}$; // initialize set of training candidates

2 **while** uncertain configuration are found during the simulations **do**

3 **for** $\{\underline{r}_i\}^* \in \{\underline{r}_i\}_j$ **do**

4 **while** simulation is not converged **do**

5 Evolve $\{\underline{r}_i\}^*$;

6 Compute the extrapolation grade γ^* of $\{\underline{r}_i\}^*$;

7 **if** $\gamma^* > \gamma_{\min}$ **then**

8 | Add $\{\underline{r}_i\}^*$ to $\mathcal{T}_{\text{cand}}$;

9 **else if** $\gamma^* > \gamma_{\max}$ **then**

10 | Abort the simulation;

11 **end**

12 **end**

13 **end**

14 **end**

15 Add the most representative configurations from $\mathcal{T}_{\text{cand}}$ to the training set and construct a new MTP using Algorithm 2.1 with $\gamma_{\text{threshold}} = \gamma_{\min}$;

Output: New MTP

3 Motoko workflow manager

The workflow described in this work is managed with the new versatile workflow manager *Motoko*, which is part of a collection of software, designed to facilitate exploration of defined parametric spaces by executing tasks and keeping records for reproducibility. *Motoko* component enables event-based as well as asynchronous-type orchestration to be written in Python. Concretely, one can execute asynchronous routines following a dependency graph, either described as asyncio Python routines, or as a collection of events triggering actions. The actions can naturally be simple routines. But they can also be pre-defined complex tasks. With every task execution, all the information relative to input parameters, software context, as well as output are preserved in a database, enabling structured queries. Such tasks can be ran locally, on distant machines, and/or on high performance computing clusters by submitting tasks to job schedulers (e.g. slurm). More details will follow in next section.

Contrary to other workflow managers [53, 54, 55, 56, 57, 58, 59], the storage is not ephemeral, i.e. every dataset produced by a task execution is kept locally on the machine that produced it (e.g. the HPC computing cluster), and/or on an object-database with remote access possibilities. It allows making queries to select tasks based on their input and/or output, during the workflow execution, but also later during results processing, with fullest possible details, aiming at enforcing reproducibility. It also allows to explore new training routes, without having to re-run the entire workflow, making exploration of new ideas flexible.

In Motoko, collections of tasks can be generated, queried, and manipulated easily. One example of an action-event relying on a collection of tasks would be described by: “*When all single-point calculations are finished, proceed to the MLIP training phase*”. In the above, the event condition will be met when no more single-point calculation tasks keep running, while the action will create a new *training* task.

When the entire workflow execution is made on a single computing resource (e.g. one laptop or one HPC cluster), all the execution and database files should be contained in the workflow directory. Making a compressed archive (tar, zip) is sufficient to pack all relevant information, enabling in depth reproducibility of executing the workflow, as well as the produced results. If one wants to export the final training set to standard repositories like *ColabFit* [43], a query to the database is sufficient. For instance, it would also be possible to export only a subset of the configurations based on the associated extrapolation grade.

3.1 Tasks

A task can be viewed as a parametric study, where the output varies according to input parameters. One key feature of the *BlackDynamite* (BD) framework, is the description and manipulation of parametric studies and spaces [60]. Therefore, each task needs to be characterized to control and monitor execution from chosen parameters. A BD task is provided a parametric space which is described by a hierarchical *yaml* file, and based on that information, BD organizes the execution of tasks and produced files while keeping record of input parameters. Chosen results are collected and organized in databases to enable complex queries. The ZODB/ZEO [61, 62] object-database serve as the storage for data and metadata, and accesses/queries to these are ensured by *BlackDynamite* API routines or with command line clients. Furthermore, BD keeps track of all files and directories so that it is almost impossible to lose produced data. BD also provides remote access to files and database content, particularly adapted to the usage

of multiple HPC computing resources. After completion of the tasks, the analysis is facilitated through automatic retrieval/conversion of data with *Numpy* arrays.

3.2 Orchestrator

A *Motoko* orchestrator is described with an asynchronous python program, to be placed in a directory containing a **motoko.yaml** file, which essentially declares the tasks, and the orchestrator main function:

```
task_managers:
  task1:
  task2:
  orchestrator: orchestrator.main
```

Here, **task1** and **task2**, are tasks, i.e. an external script (usually a set of python functions) that serves as a template to create actual executions. The orchestrator can start/stop new executions of any declared task. The orchestrator role, is to decide when to execute new tasks, in reaction to results of others. For example, by launching specific instances of **task2** by choosing its parameters based on the output of **task1** instances.

The asynchronous orchestrator is usually placed in a python script called **orchestrator.py**, while **main** is the function starting the workflow. The folder structure of a Motoko workflow then looks as follows:

```
workflow/
  orchestrator.py
  motoko.yaml
  task1/
    run.sh
    doit.py
    bd.yaml
  task2/
    run.sh
    doit.py
    bd.yaml
```

Here, the **run.sh** files are bash scripts calling the Python functions of the corresponding task provided in the **doIt.py** files. The asynchronous execution can be demanded with the command **motoko orchestrator start** from the **workflow/** folder.

In the following sections, details are provided on how to declare the entire Motoko workflow, from tasks up to the asynchronous routines realizing the orchestration for our MLIP training.

4 Autopot workflow

For MLIPs conceived with active machine-learning, it is neither necessary nor desired to explore the entire parametric space (we cannot compute all the energies for an infinite number of configurations). Instead, adequate selections of training configurations should be performed dynamically during the global workflow execution. The goal is to find a small, affordable set of training configurations to achieve the desired accuracy. *AutoPot* is a workflow orchestrator, following Motoko's framework, that realizes active learning as described in Section 2. Below is described the definition of the tasks associated with the active learning protocols described earlier.

4.1 Tasks

Autopot connects four tasks (**select**, **md_select**, **sp_calc**, and **train**) which will be executed in agreement with the *uncertainty quantification* obtained from configurations. In more details:

1. **select**: *Selection of configurations* by evaluating the extrapolation grade. It follows Algorithm 2.1 which will execute the **select-add** command from MLIP-2 to populate a file with configurations on which to perform a single-point calculation.
2. **md_select**: *Molecular dynamics simulations* used to select configurations. It runs Algorithm 2.2 with Langevin dynamics, as implemented in ASE [63].
3. **sp_calc**: *Single point calculation* evaluating the energy, forces, and stresses, for a given atomic configuration. Two versions of **sp_calc** have been implemented, one that uses the **EAMCalculator** from ASE as a reference for testing. The other version runs a VASP calculation.
4. **train**: *Training the MLIP* that minimizes the loss function (4) for a given training set. Such a task executes the command **mlp train** from MLIP-2.

These four tasks are described using BlackDynamite’s framework, and the parameter space associated with each of these tasks is given in a `.yaml` file, as shown in Figure 2. The parametric space is two-fold: 1) the job space describes the physical quantities or model properties controlling the task. 2) the run space provides the opportunity to describe parameters regarding the actual execution. For instance, the temperature is a job parameter while the slurm options or the MD software are usually run parameters. In summary, selections (`select` or `md_select`) identify the uncertain configurations, and single-point calculations (`sp_calc`) compute the energies, forces, and stresses, of selected configurations in order to update the training set. Each time the training set is determined, a `train` task will produce a new MLIP by minimizing the loss function. This sequence of task executions is performed until no new uncertain configuration is found/created from the selection tasks.

| <code>task: md_select</code> | <code>task: sp_calc</code> | <code>task: train</code> |
|---|---|--|
| <pre>task: select job: grade: float training_candidate_sets: list pot_fname: str ts_fname: str atom_types: str run: slurm_options: list</pre> | <pre>job: cfg_fname: str pot_fname: str ts_fname: str atom_types: str md_args: dict select_args: dict run: md_software: str slurm_options: list</pre> | <pre>job: pot_fname: str ts_fname: str sp_calc_ids: list atom_types: str train_args: dict run: slurm_options: list</pre> |

Figure 2: `.yaml` files of the tasks implemented in AutoPot. For the `sp_calc` version that runs a VASP calculation, `pot_fname` corresponds to the INCAR file. For the `train` tasks, the id’s of `sp_calc` tasks can be provided as a list in order to add the calculated energies, forces, and stresses, from those `sp_calc` tasks to the training set.

4.2 Orchestration

In order to complete the workflow description, the orchestration is given as an asynchronous python program, to be placed in a directory containing a `motoko.yaml` file. This file registers the tasks, as well as the orchestrator’s main function:

```
task_managers:
  select:
  md_select:
  sp_calc:
  train:
orchestrator: orchestrator.main
```

Essentially, the workflow is described with python functions that are declared as `async`, making them not necessarily executed immediately. The obvious reason being that the orchestrator may trigger the creation of tasks, the execution scheduling, and finally the storage of results which will take time. Before the workflow can get a chance to resume execution, the `async` declaration offers it the possibility to treat other orchestration duties asynchronously. An example of such a routine would be:

```
@event
async def spawn_sp_calc_task(workflow, cfg_fnames):
    created_calc_runs = await workflow.sp_calc.createTask(cfg_fname=cfg_fnames)
    return created_calc_runs
```

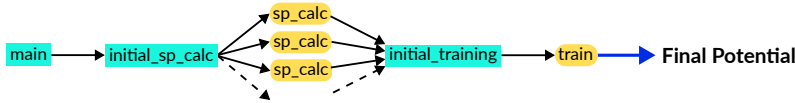
In the example above, configuration filenames are used to create one `sp_calc` task per configuration with the `createTask` call. The `await` keyword specifies that this is an asynchronous call which needs another execution to finish before resuming execution of the orchestration. After completion, the return variable `created_calc_runs` is a collection of executed (BD) tasks that may be queried for properties, state, results, or even remotely produced files.

We have decomposed the full AutoPot workflow into the three stages shown in Figure 3, each of them taking an initial training set as input and return a trained potential:

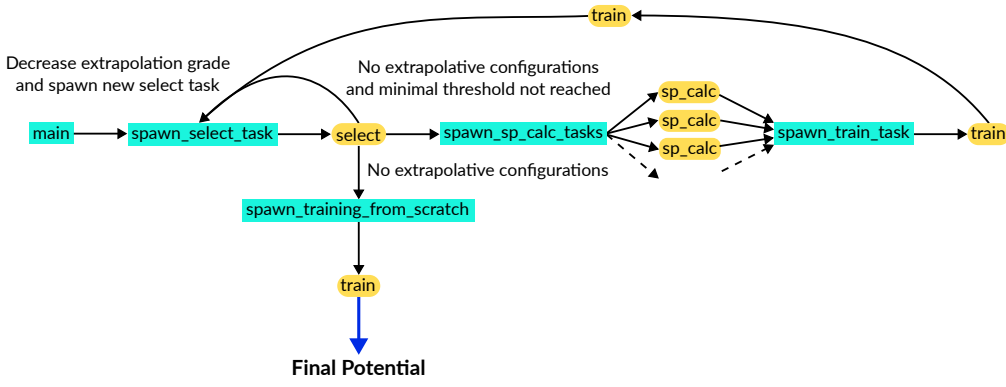
- (a) `calculate_ts` produces a training set from an initial set of configurations.
- (b) `select_and_calc_ts` will sample the training set from a training candidate set based on a varying extrapolation threshold (Algorithm 2.1).
- (c) `md_select_and_calc_ts` will sample the training set from MD simulations on a chosen set of configurations (Algorithm 2.2).

Once uncertain configurations are found in any of the selection stages, **select** and **md_select**, corresponding **sp_calc** runs will be spawned. Again, when all **sp_calc** runs are finished, a new **train** run will add all new configurations to the training set and retrain the potential.

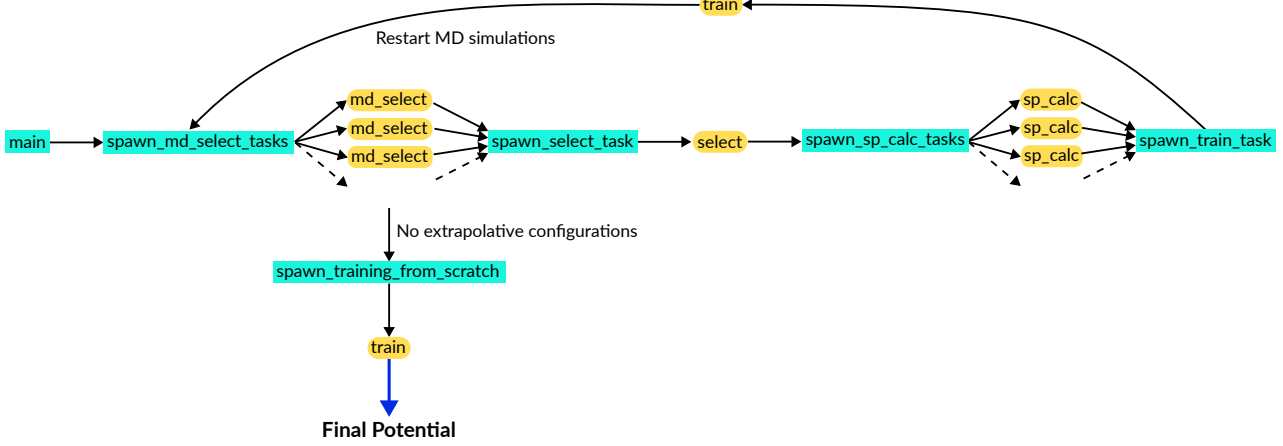
(a) **calculate_ts**:



(b) **select_and_calc_ts**:



(c) **md_select_and_calc_ts**:



async routines task executions

Figure 3: Workflow stages implemented in AutoPot. The cyan boxes are *async* routines given in the file **orchestrator.py**, while yellow boxes refer to *task* executions

The **select** stage could produce an unnecessarily large number of training configurations for very large training candidate sets when selecting all configurations above a small extrapolation grade between 1 and 2 at once (cf. Section 2.3). To avoid this, we iteratively spawn **select** tasks, first with a very large extrapolation threshold (e.g. $> 100\,000$), then with some smaller extrapolation threshold (e.g. $> 10\,000$), etc., and finally with an extrapolation threshold between 1 and 2 (corresponding to accurate extrapolation). This ensures that configurations selected for training are sufficiently distinct from each other.

The three stages can be called standalone or in sequence from the orchestrator. The behavior of the full orchestrator, as seen in Figure 7, can be controlled by the following arguments:

```
--potential 08.mtp           interatomic potential to start with
--fresh_potential 08.mtp      untrained interatomic potential to be used for training from scratch after collecting all training configurations
--training_set ts.cfg         initial training set
```

```
--calculate_ts      calculate the initial training set and train the potential on it
--atom_types W=0,Ta=1,..., -a W=0,Ta=1,...
               mapping of atomic types to numbers according to convention used in the potential code
--select           pre-select configurations from the candidate set
--grades [10000 1000 100 ...], -g [10000 1000 100 ...]
               Maximum extrapolation grades above which iteratively configurations are selected for training
--training_candidate_set tcs.cfg
               Set with the training candidates
--md_select        select configurations from MD simulations
--md_configurations configurations.xyz
               file with atomic configurations on which to run the MD simulations.
               If not given, run MD on each configuration from the training set
```

For instance, by running the workflow with the command line:

```
motoko orchestrator start --potential 08.mtp --training_set init_training_cfgs.xyz --calculate_ts --atom_types Mo=0 \
--md_select --md_configurations md_cfgs.xyz
```

We have built in some flexibility by allowing to either choose **--select** and **--md_select** individually, or a combination of both. If both options are chosen, then the workflow always starts with the **select** stage. When all MD simulations are finished without triggering new single-point calculations, the orchestrator will terminate. After completion of the workflow, the MTP file and training set from the last **train** task can be accessed with the following python script:

```
wf = Workflow("motoko.yaml")

# get the last task execution run
last_run = wf.train.connect().runs[wf.train.connect().runs_counter - 1]

# get the running directory for that run
run_path = os.path.join(
    wf.train.study_dir, f"BD-train-runs/run-{last_run['id']}")

# obtain a full path name for the potential and training set
mtp_fname = os.path.join(
    run_path, last_run.train_args["trained_pot_name"])
)
ts_fname = os.path.join(
    run_path, last_run.train_args["ts_name"])
)
```

5 AutoPot in production mode

We now test AutoPot in production mode by constructing two MTPs, one for bcc W, and one for Mo-Ta random alloys. We benchmark the trained potentials on material properties relevant for nanoscale plasticity, such as elastic constants, stacking fault energies, and several key properties of dislocations. There is plenty of DFT data available for this combination of materials and properties which makes it ideal for benchmarking.

We first describe the details of the training protocol that are the same for both potentials. As an ab initio model we use DFT with a setup close to the one used in [28]: we employ the Vienna Ab initio Simulation Package (VASP) [64] with plane-wave basis sets, the projector-augmented wave (PAW) pseudopotential method [65, 66], and the PBE method [67] to calculate the exchange-correlation functional; we further use an energy cutoff of 400 eV, a Gaussian smearing of 0.08 eV, and a minimum k -point spacing of 0.15 \AA^{-1} . Electronic relaxation is performed using the preconditioned minimal residual method. A configuration is considered as converged when the energy difference between two iterations is less than 5×10^{-7} eV.

As an interatomic potential, we use an MTP of level 16 with the cut-off radius set to 5 \AA . Unless specified otherwise, we run AutoPot using the default options given in the previous section. The examples presented in this section have been run on the Vienna Scientific Cluster (VSC-5) provided by the Austrian Scientific Computing (ASC) facilities.

5.1 MTP for W

We choose to train our potential on two types of configurations, bulk configurations with 54 atoms per supercell, and configurations containing a $1/4 [111]$ stacking fault with 72 atoms per supercell. For each type of configuration, we first create a very large set of training candidates with 10 000 samples in their ground state. A Cauchy strain is applied to each sample, extracted from a uniform distribution with the minimum and maximum strain components set to $\pm 2 \text{ \%}$. Moreover, the atomic positions of each strained sample are randomly perturbed using a Gaussian distribution with a standard deviation of 0.02 \AA .

We start from a training set containing 20 configurations (10 bulk and 10 stacking fault configurations). We then perform a pre-selection of training configurations from the training candidate set using the **select** task. That is, we iteratively add configurations with high extrapolation grades by gradually lowering the threshold (cf. Algorithm 2.1) until the extrapolation grades of all configurations in the training candidate set are < 2 . Afterwards, we sample the

remaining training configurations from two MD trajectories starting from one bulk and one stacking fault configuration in the ground state.

In Figure 4, we show the evolution of the training set size as a function of the selection iteration. The total number of configurations selected by AutoPot is 123. Almost all of the configurations (118) are added during the third iteration of the pre-selection phase (when $\gamma_{\text{threshold}} = 10\,000$). From the MD simulations, only a small number of 5 configurations is selected for training. This is somewhat expected and demonstrates the correct functioning of the AutoPot workflow: configurations appearing in MD simulations at 100 K are not too far from the ground state and are already sufficiently well covered by the large training candidate set of 10 000 samples per configuration type.

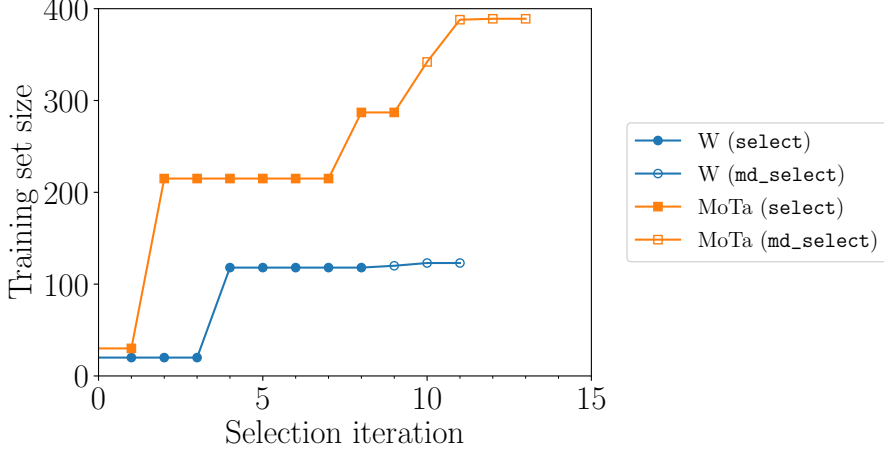


Figure 4: Evolution of training set size of the MTPs for W and Mo-Ta as a function of the selection iteration

The MTP training errors are shown in Table 2. The errors are well within the range known to be sufficient for MTPs to predict elastic and defect properties in unary metals with near-DFT accuracy, i.e., of the order of 1 meV for per-atom energies, of the order of 10 meV/Å for forces, and of the order of 10^{-1} GPa for stresses (cf. e.g., [28, 68]).

| MTP | Energy MAE [meV/atom] | Energy RMSE [meV/atom] | Force MAE [meV/Å] | Force RMSE [meV/Å] | Stress MAE [GPa] | Stress RMSE [GPa] |
|------|--------------------------|---------------------------|----------------------|-----------------------|---------------------|----------------------|
| W | 0.50 | 0.78 | 33.5 | 64.0 | 0.064 | 0.216 |
| MoTa | 2.18 | 2.91 | 39.0 | 76.2 | 0.090 | 0.291 |

Table 1: Mean absolute error (MAE) and root mean square error (RMSE) of the MTPs for W and MoTa

The MTP is then benchmarked on various properties relevant for studying dislocation plasticity, namely, the lattice constant, elastic constants, and the 1/4[111] unstable stacking fault energy; the simulation details for all considered properties are given in Appendix B. Overall, the agreement with DFT is very good, as shown in Table 2. The MTP error on all quantities is less than 10 %, comparable to other highly accurate MLIPs for W (e.g., [28, 69]).

| Method | a_0 [Å] | C_{11} [GPa] | C_{12} [GPa] | C_{44} [GPa] | Π^{usf} [mJ/m ²] |
|--------|--------------|-------------------|-------------------|-------------------|--|
| MTP | 3.172 | 551.4 | 200.0 | 139.9 | 1872.3 |
| DFT | 3.168 | 545.3 | 211.5 | 145.5 | 1772.7 |

Table 2: Comparison of the elastic properties and the 1/4[111] unstable stacking fault energy of the MTP for W to DFT. The DFT values of the elastic properties are taken from [28], the DFT value of the stacking fault energy is taken from [70]

Next, we benchmark the MTP on properties of 1/2⟨111⟩ screw dislocations by comparing our "AutoPot MTP" to the MTP of Hodapp and Shapeev [28] that has been trained on dislocation cores that have been extracted on-the-fly while running a relaxation. Training a MLIP on all relevant neighborhoods appearing in a simulation is the most rigorous way to make the simulation using that MLIP as close as possible to a large-scale DFT simulation. Therefore, we denote the MTP of Hodapp and Shapeev [28] as the *reference MTP* in the following.

Upon relaxing the dislocation, we inspect the differential displacements around the dislocation core. The relaxed core structure is non-polarized (Figure 5 (a)) in agreement with the reference MTP and DFT (cf. [28], Figure 3). We then compute the energy difference between the relaxed configuration and the initial configuration in which the dislocation has been inserted using the elastic displacement field of a screw dislocation. The MTP result (-0.158 eV per Burgers vector) deviates only by a few percent from the reference MTP result (-0.166 eV per Burgers vector).

We finally calculate the minimum energy path (MEP) of the screw dislocation while crossing the Peierls valley. Again, the MEP of our new MTP, constructed using AutoPot, agrees very well with the MEP from the reference MTP; the difference in the Peierls barrier of our MTP (0.081 eV) is within a few percent from the reference MTP (0.088 eV). This is remarkable given the small size of the training set containing only 123 configurations, thanks to active learning selecting only the most distinct configuration to be used for training.

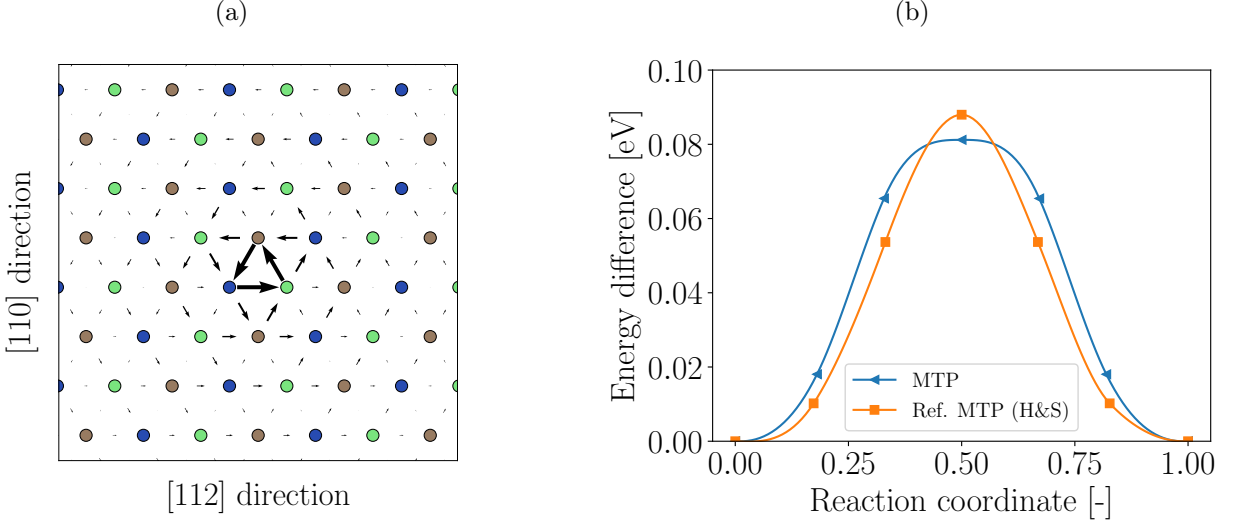


Figure 5: (a) Differential displacement plot [71] of the relaxed dislocation core using the MTP for W. (b) Minimum energy path of the MTP for W and of the reference MTP from Hodapp and Shapeev [28] that has been trained on configurations containing the dislocation cores that appeared during the NEB calculations

5.2 MTP for Mo-Ta random alloys

We compose the training set for Mo-Ta of the same types of configurations as for the W potential, namely, bulk configurations with 54 atoms per supercell, and configurations containing a 1/4 [111] stacking fault with 72 atoms per supercell. For each configuration type, we create a set of training candidates with 30 000 samples using the lattice constant for the equiatomic alloy. The alloy composition of each sample is drawn from a Dirichlet distribution over the entire composition space. A Cauchy strain is applied to each sample which is extracted from a uniform distribution with the minimum and maximum strain components set to $\pm 3\%$. The atomic positions of each sample are randomly perturbed using a Gaussian distribution with a standard deviation of 0.02 \AA .

Our initial training set contains 30 configurations (5 bulk and 5 stacking fault configurations at 100 % Mo, equiatomic composition, and 100 % Ta). Pre-selection of training configurations from the candidate set is performed in the same way as for the W potential. To test whether AutoPot is able to handle sampling from many MD trajectories in parallel, we run MD simulations on *each* of the configurations that is contained in the training set after the pre-selection phase.

The evolution of the training set size as a function of the selection iteration is shown in Figure 4. The total number of configurations selected by AutoPot is 389. Most of the configurations (287) are added during the second and last iteration of the pre-selection phase (when $\gamma_{\text{threshold}} = 100\,000$, and $\gamma_{\text{threshold}} = 2$). Still a considerable amount of 102 configurations is selected during the MD simulations. This can be attributed to the large number of MD simulations (287) but also to chemistry effects altering the dynamics of atoms, which is difficult to capture a priori before running a simulation (cf. [16]).

The MTP training errors are given in Table 2. All errors are well within the tolerances that are known to be sufficient for MTPs being able to predict elastic and defect properties in random alloys with an accuracy close to that of DFT, i.e., of the order of 1 meV for per-atom energies, of the order of 10 meV/\AA for forces, and of the order of 10^{-1} GPa for stresses (cf., e.g., [16, 51, 52]).

The MTP is then benchmarked on various properties relevant for studying dislocation plasticity, namely, the lattice constant, elastic constants, and the 1/4 [111] unstable stacking fault energy; the simulation details for all considered properties are given in Appendix B. Overall, the agreement with DFT over the entire composition space is very good, as shown in Table 2. The MTP error on all quantities is less than 10 %, comparable to other accurate MLIPs for random alloys (e.g., [72, 73, 74]).

Overall, our results confirm the excellent accuracy of previous MTPs for alloys across the entire composition space. However, those previous MTPs have been tediously constructed by actively sampling the training configurations from sequential MD simulations using semi-automated workflows (cf. [51]). With AutoPot, constructing highly accurate MTPs that are stable over a wide configuration and chemical space is now possible fully automatically within a couple of hours, and with minimal input required by the user.

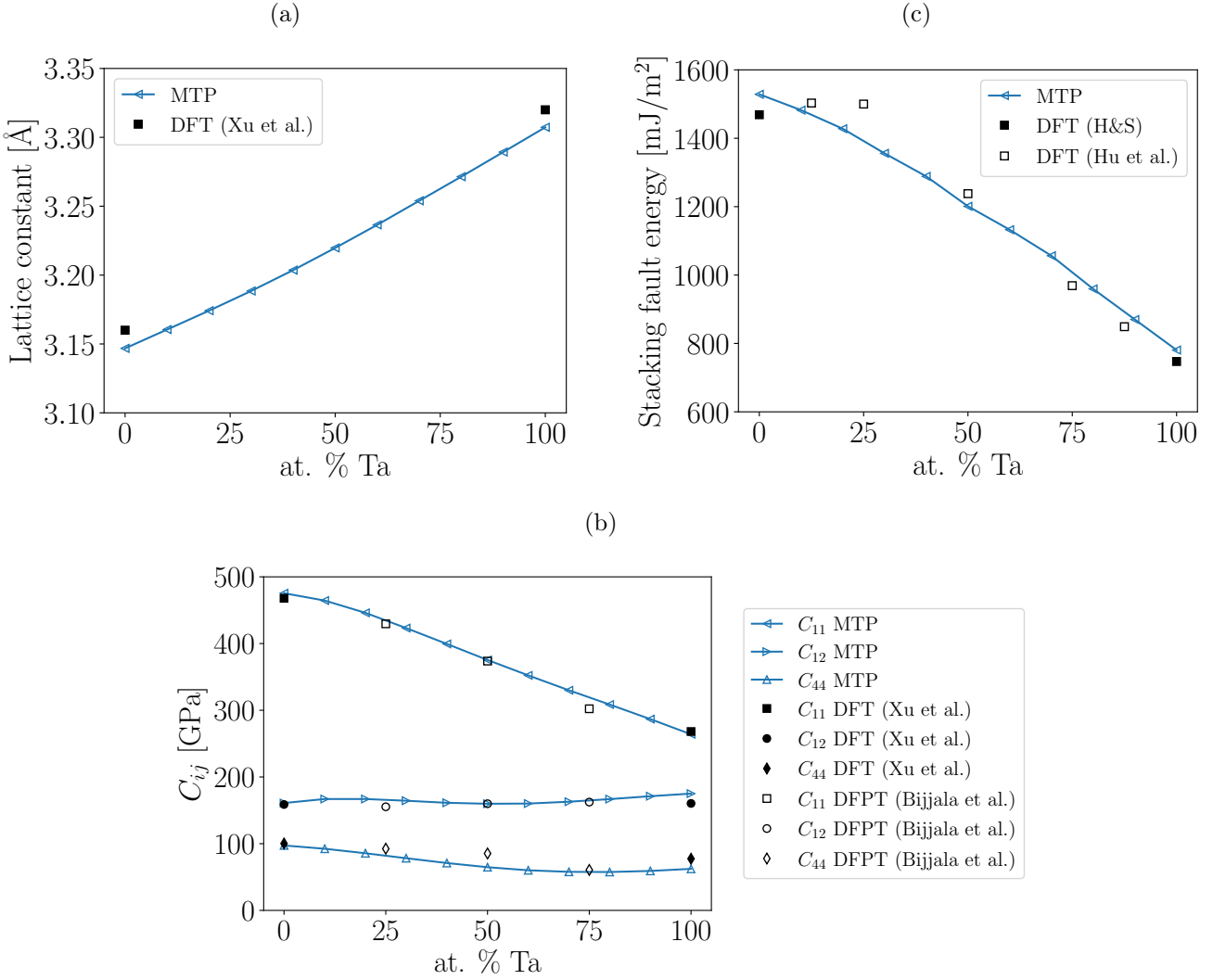


Figure 6: Comparison of the elastic properties and the 1/4[111] unstable stacking fault energy of the MTP for Mo-Ta to DFT. The DFT values are taken from Xu et al. [70], Hu et al. [75], Hodapp and Shapeev [51], and Biju et al. [76]

6 Concluding remarks

In the present work, we have introduced AutoPot, a software for constructing machine-learning potentials (MLIPs) in an automated fashion. MLIPs aim at bringing quantitative accuracy of quantum mechanics to the atomic scale, but reaching their full potential is still hampered by constructing proper training data, in particular for multicomponent systems, or systems with complex quantum-mechanical interactions, such as magnetism. Advanced learning algorithms like active learning or fine-tuning can substantially reduce the amount of training data and improve the accuracy but require sophisticated protocols to streamline the construction of MLIP. AutoPot alleviates designing such protocols using the BlackDynamite framework that manages parametric studies in a highly automated and parallelized fashion, supported by the Motoko workflow manager that manages interactions between the studies.

One of the key advantages of basing AutoPot on BlackDynamite is the possibility of allowing tasks to be implemented as Python scripts without the need of writing parsers. As such it can easily be extended to include other MLIP software, ab initio codes, etc. It therefore provides the community with a flexible and versatile tool for streamlining the construction of MLIPs. Moreover, it can serve as a framework for benchmarking learning protocols for MLIPs. This is, in our view, a critically understudied part of constructing MLIPs, as benchmarking MLIPs is mostly done by comparing their accuracy on pre-defined datasets.

The present version of AutoPot selects training configurations based on the D-optimality criterion. The D-optimality criterion is an error indicator and guarantees a stable potential but is not necessarily a good quantification of the true error. There exist more advanced algorithms, such as sampling from uncertainty-driven simulations [77], re-calibration of uncertainties [78, 79], or property-specific error metrics [21], which could be integrated in future versions of AutoPot.

While our first version of AutoPot is presented as a standalone program, our vision is to interface it with a molecular dynamics code, where training configurations can be constructed and submitted on-the-fly, thanks to the splitting of

job submission and workflow orchestration. Developing such an interface will be part of future work.

Finally, we remark that the methodology developed for AutoPot is not limited to MLIPs but could be applied to other learning tasks, such as actively learning continuum models from atomistic data (e.g., [80]).

7 Data availability

BlackDynamite, Motoko, and AutoPot are on gitlab [34, 46, 47].

8 Acknowledgments

We thank Franco Moitzi and Daniil Khodachenko for their initial testing of AutoPot and helpful suggestions on improving the documentation.

MH gratefully acknowledges the financial support by the Austrian Federal Ministry for Labour and Economy and the National Foundation for Research, Technology and Development and the Christian Doppler Research Association.

Appendix

A Autopot orchestration diagram

The orchestration diagram of the full workflow implemented in AutoPot is shown in Figure 7.

B Simulation details

Below, we give the simulation details of all the calculations from Section 5. Setting up the simulations has been done in Python with the help of ASE [63], matscipy [81], and MlipPyKit (gitlab.com/mhodapp/mlippykit).

Ground state To compute the material’s ground state, we minimize the total energy of the primitive cell with respect to the lattice constant using the Nelder-Mead simplex algorithm as implemented in SciPy. We consider a configuration as converged when the difference between the solutions for two subsequent iterations is less than 10^{-10} Å. For computing the lattice constants of the alloys, we use a supercell of 2 000 atoms with the Mo and Ta atoms randomly distributed corresponding to a given composition.

Elastic constants We compute the elastic constants by linearly regressing the stresses as a function of the strains around the ground state using the `fit_elastic_constants` function from matscipy. For computing the elastic constants of the alloys, we again use a supercell of 2 000 atoms with the Mo and Ta atoms randomly distributed corresponding to a given composition.

1/4[111] stacking fault energy We first create a rectangular supercell with the directions corresponding to the axes set to $[11\bar{2}]$, $[\bar{1}10]$, and $[111]$, respectively. This configuration is denoted by $\{\underline{r}^i\}_{\text{bulk}}$. We now translate half of the atoms in $\{\underline{r}^i\}_{\text{bulk}}$ by one Burgers vector in the $[111]$ direction to create the stacking fault; in addition, we apply a shear displacement of half a Burgers vector to the cell vectors such that there will be only one stacking fault per supercell. This configuration is denoted by $\{\underline{r}^i\}_{\text{sf}}$. The stacking fault energy is the difference between the total energy of both configurations divided by the area of the fault plane A

$$\Pi^{\text{sf}} = \frac{\Pi(\{\underline{r}^i\}_{\text{sf}}) - \Pi(\{\underline{r}^i\}_{\text{bulk}})}{A}.$$

For computing Π^{sf} of a random alloy, we use supercells of about 100 000 atoms, which practically removes any spurious size effects (cf. [16]).

Dislocation core relaxation The dislocation is inserted in a cylindrical configuration with a radius of 35 Å times the magnitude of the Burgers vector. We constrain the positions of the outermost atoms that have a radial distance to the boundary of two times the cut-off radius to the linear elastic solution of a screw dislocation. This leaves about 5 000 free atoms that are allowed to relax. Energy minimization is performed using the Fast Inertial Relaxation Engine [82], as implemented in ASE. We consider an energy minimization as converged when the maximum absolute force on an atom is less than 10^{-3} eV/Å.

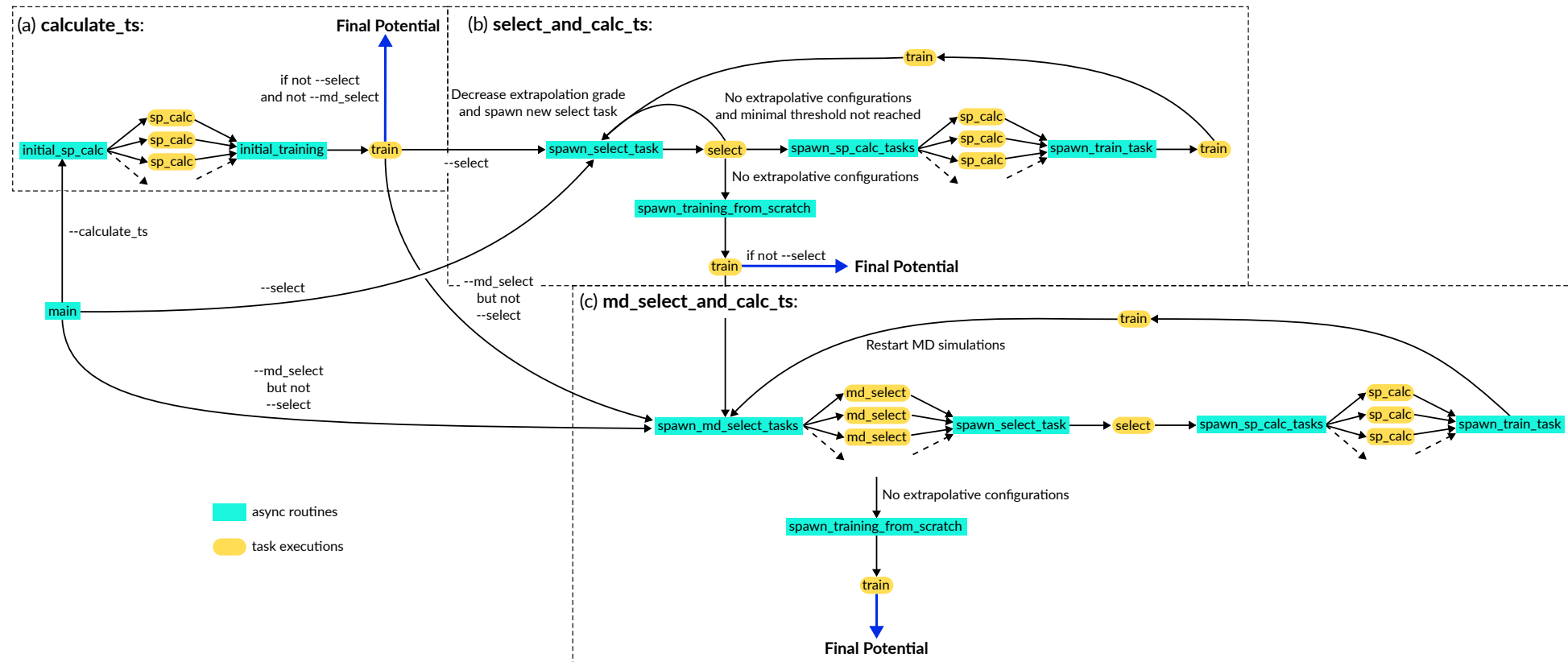


Figure 7: Full workflow implemented in AutoPot

NEB calculations The NEB calculations are performed using the same configuration as for the dislocation core relaxation. We use the climbing NEB method of Henkelman and Jónsson [83] with seven images. The images are created by linearly interpolating between two configurations that differ in the position of the dislocation by one Peierls distance.

References

- [1] Jörg Behler and Michele Parrinello. “Generalized Neural-Network Representation of High-Dimensional Potential-Energy Surfaces”. In: *Physical Review Letters* 98.14 (Apr. 2, 2007), p. 146401. DOI: [10.1103/PhysRevLett.98.146401](https://doi.org/10.1103/PhysRevLett.98.146401).
- [2] Albert P. Bartók et al. “Gaussian Approximation Potentials: The Accuracy of Quantum Mechanics, without the Electrons”. In: *Physical Review Letters* 104.13 (Apr. 1, 2010), p. 136403. DOI: [10.1103/PhysRevLett.104.136403](https://doi.org/10.1103/PhysRevLett.104.136403).
- [3] A.P. Thompson et al. “Spectral neighbor analysis method for automated generation of quantum-accurate interatomic potentials”. In: *Journal of Computational Physics* 285 (Mar. 2015), pp. 316–330. DOI: [10.1016/j.jcp.2014.12.018](https://doi.org/10.1016/j.jcp.2014.12.018).
- [4] Alexander V. Shapeev. “Moment Tensor Potentials: A Class of Systematically Improvable Interatomic Potentials”. In: *Multiscale Modeling & Simulation* 14.3 (Jan. 2016), pp. 1153–1173. DOI: [10.1137/15M1054183](https://doi.org/10.1137/15M1054183).
- [5] Linfeng Zhang et al. “Deep Potential Molecular Dynamics: A Scalable Model with the Accuracy of Quantum Mechanics”. In: *Physical Review Letters* 120.14 (Apr. 4, 2018), p. 143001. DOI: [10.1103/PhysRevLett.120.143001](https://doi.org/10.1103/PhysRevLett.120.143001).
- [6] Ralf Drautz. “Atomic cluster expansion for accurate and transferable interatomic potentials”. In: *Physical Review B* 99.1 (Jan. 8, 2019), p. 014104. DOI: [10.1103/PhysRevB.99.014104](https://doi.org/10.1103/PhysRevB.99.014104).
- [7] G. P. Purja Pun et al. “Physically informed artificial neural networks for atomistic modeling of materials”. In: *Nature Communications* 10.1 (May 28, 2019), p. 2339. DOI: [10.1038/s41467-019-10343-5](https://doi.org/10.1038/s41467-019-10343-5).
- [8] Oliver T. Unke et al. “Machine Learning Force Fields”. In: *Chemical Reviews* 121.16 (Aug. 25, 2021), pp. 10142–10186. DOI: [10.1021/acs.chemrev.0c01111](https://doi.org/10.1021/acs.chemrev.0c01111).
- [9] Simon Batzner et al. “E(3)-equivariant graph neural networks for data-efficient and accurate interatomic potentials”. In: *Nature Communications* 13.1 (May 4, 2022), p. 2453. DOI: [10.1038/s41467-022-29939-5](https://doi.org/10.1038/s41467-022-29939-5).
- [10] Ilyes Batatia et al. “MACE: Higher Order Equivariant Message Passing Neural Networks for Fast and Accurate Force Fields”. In: *Advances in Neural Information Processing Systems*. Ed. by S. Koyejo et al. Vol. 35. Curran Associates, Inc., 2022, pp. 11423–11436.
- [11] Zheyong Fan et al. “GPUMD: A package for constructing accurate machine-learned potentials and performing highly efficient atomistic simulations”. In: *The Journal of Chemical Physics* 157.11 (Sept. 21, 2022), p. 114801. DOI: [10.1063/5.0106617](https://doi.org/10.1063/5.0106617).
- [12] M Hodapp and A Shapeev. “Equivariant tensor network potentials”. In: *Machine Learning: Science and Technology* 5.3 (Sept. 1, 2024), p. 035075. DOI: [10.1088/2632-2153/ad79b5](https://doi.org/10.1088/2632-2153/ad79b5).
- [13] Junjie Wang et al. “E(n)-Equivariant cartesian tensor message passing interatomic potential”. In: *Nature Communications* 15.1 (Sept. 1, 2024), p. 7607. DOI: [10.1038/s41467-024-51886-6](https://doi.org/10.1038/s41467-024-51886-6).
- [14] Bohayra Mortazavi. “Recent Advances in Machine Learning-Assisted Multiscale Design of Energy Materials”. In: *Advanced Energy Materials* 15.9 (Mar. 2025), p. 2403876. DOI: [10.1002/aenm.202403876](https://doi.org/10.1002/aenm.202403876).
- [15] J. Byggmästar, K. Nordlund, and F. Djurabekova. “Modeling refractory high-entropy alloys with efficient machine-learned interatomic potentials: Defects and segregation”. In: *Physical Review B* 104.10 (Sept. 3, 2021), p. 104101. DOI: [10.1103/PhysRevB.104.104101](https://doi.org/10.1103/PhysRevB.104.104101).
- [16] Franco Moitzi et al. “Ab initio framework for deciphering trade-off relationships in multi-component alloys”. In: *npj Computational Materials* 10.1 (July 16, 2024), p. 152. DOI: [10.1038/s41524-024-01342-2](https://doi.org/10.1038/s41524-024-01342-2).
- [17] Keke Song et al. “General-purpose machine-learned potential for 16 elemental metals and their alloys”. In: *Nature Communications* 15.1 (Nov. 25, 2024), p. 10208. DOI: [10.1038/s41467-024-54554-x](https://doi.org/10.1038/s41467-024-54554-x).
- [18] Lei Zhang et al. “Atomistic fracture in bcc iron revealed by active learning of Gaussian approximation potential”. In: *npj Computational Materials* 9.1 (Dec. 8, 2023), p. 217. DOI: [10.1038/s41524-023-01174-6](https://doi.org/10.1038/s41524-023-01174-6).
- [19] Kazuma Ito et al. “Machine learning interatomic potential with DFT accuracy for general grain boundaries in α -Fe”. In: *npj Computational Materials* 10.1 (Nov. 13, 2024), p. 255. DOI: [10.1038/s41524-024-01451-y](https://doi.org/10.1038/s41524-024-01451-y).
- [20] Shuyao Lin et al. “Machine-learning potentials for nanoscale simulations of tensile deformation and fracture in ceramics”. In: *npj Computational Materials* 10.1 (Apr. 2, 2024), p. 67. DOI: [10.1038/s41524-024-01252-3](https://doi.org/10.1038/s41524-024-01252-3).

[21] Yunsheng Liu and Yifei Mo. "Learning from models: high-dimensional analyses on the performance of machine learning interatomic potentials". In: *npj Computational Materials* 10.1 (July 20, 2024), p. 159. DOI: [10.1038/s41524-024-01333-3](https://doi.org/10.1038/s41524-024-01333-3).

[22] Linus C. Erhard et al. *How Realistic are Idealized Copper Surfaces? A Machine Learning Study of Rough Copper-Water Interfaces*. Sept. 22, 2025. DOI: [10.48550/arXiv.2509.17833](https://doi.org/10.48550/arXiv.2509.17833). arXiv: [2509.17833\[cond-mat\]](https://arxiv.org/abs/2509.17833).

[23] Fei Shuang et al. "Modeling extensive defects in metals through classical potential-guided sampling and automated configuration reconstruction". In: *npj Computational Materials* 11.1 (May 3, 2025), p. 118. DOI: [10.1038/s41524-025-01599-1](https://doi.org/10.1038/s41524-025-01599-1).

[24] Burr Settles. "Active Learning Literature Survey". In: (2009).

[25] Evgeny V. Podryabinkin and Alexander V. Shapeev. "Active learning of linearly parametrized interatomic potentials". In: *Computational Materials Science* 140 (Dec. 2017), pp. 171–180. DOI: [10.1016/j.commatsci.2017.08.031](https://doi.org/10.1016/j.commatsci.2017.08.031).

[26] Linfeng Zhang et al. "Active learning of uniformly accurate interatomic potentials for materials simulation". In: *Physical Review Materials* 3.2 (Feb. 25, 2019), p. 023804. DOI: [10.1103/PhysRevMaterials.3.023804](https://doi.org/10.1103/PhysRevMaterials.3.023804).

[27] Jonathan Vandermause et al. "On-the-fly active learning of interpretable Bayesian force fields for atomistic rare events". In: *npj Computational Materials* 6.1 (Mar. 18, 2020), p. 20. DOI: [10.1038/s41524-020-0283-z](https://doi.org/10.1038/s41524-020-0283-z).

[28] M Hodapp and A Shapeev. "In operando active learning of interatomic interaction during large-scale simulations". In: *Machine Learning: Science and Technology* 1.4 (Dec. 1, 2020), p. 045005. DOI: [10.1088/2632-2153/aba373](https://doi.org/10.1088/2632-2153/aba373).

[29] Evgeny V. Podryabinkin et al. "Nanohardness from First Principles with Active Learning on Atomic Environments". In: *Journal of Chemical Theory and Computation* 18.2 (Feb. 8, 2022), pp. 1109–1121. DOI: [10.1021/acs.jctc.1c00783](https://doi.org/10.1021/acs.jctc.1c00783).

[30] Bowen Deng et al. *Overcoming systematic softening in universal machine learning interatomic potentials by fine-tuning*. May 11, 2024. DOI: [10.48550/arXiv.2405.07105](https://doi.org/10.48550/arXiv.2405.07105). arXiv: [2405.07105\[cond-mat\]](https://arxiv.org/abs/2405.07105[cond-mat]).

[31] Alexey S. Kotykhov et al. "Actively trained magnetic moment tensor potentials for mechanical, dynamical, and thermal properties of paramagnetic CrN". In: *Physical Review B* 111.9 (Mar. 27, 2025), p. 094438. DOI: [10.1103/PhysRevB.111.094438](https://doi.org/10.1103/PhysRevB.111.094438).

[32] FAIR Principles. <https://www.go-fair.org/fair-principles/>.

[33] MLOps Tools You Need to Know in 2024. <https://www.datacamp.com/blog/top-mlops-tools>.

[34] BlackDynamite. <https://gitlab.com/ganciaux/blackdynamite>. Apr. 2024.

[35] Bamboost. <https://bamboost.ch/>.

[36] Productive parallel programming in Python. <https://parsl-project.org/>.

[37] Dynamic, crash-proof AI orchestration. <https://flyte.org/>.

[38] Materials Project. <https://next-gen.materialsproject.org/>.

[39] The Materials Cloud Team. *Materials Cloud*. <https://www.materialscloud.org/home>. Text.

[40] Giovanni Pizzi et al. "AiiDA: automated interactive infrastructure and database for computational science". In: *Computational Materials Science* 111 (2016), pp. 218–230. DOI: <https://doi.org/10.1016/j.commatsci.2015.09.013>.

[41] Custodian. <http://materialsproject.github.io/custodian/>.

[42] E. B. Tadmor et al. "The Potential of Atomistic Simulations and the Knowledgebase of Interatomic Models". In: *JOM* 63.7 (July 2011), pp. 17–17. DOI: [10.1007/s11837-011-0102-6](https://doi.org/10.1007/s11837-011-0102-6).

[43] Joshua A. Vita et al. "ColabFit exchange: Open-access datasets for data-driven interatomic potentials". In: *The Journal of Chemical Physics* 159.15 (Oct. 21, 2023), p. 154802. DOI: [10.1063/5.0163882](https://doi.org/10.1063/5.0163882).

[44] Kiran Mathew et al. "Atomate: A high-level interface to generate, execute, and analyze computational materials science workflows". In: *Computational Materials Science* 139 (2017), pp. 140–152. DOI: <https://doi.org/10.1016/j.commatsci.2017.07.030>.

[45] Jan Janssen et al. "pyiron: An integrated development environment for computational materials science". In: *Computational Materials Science* 163 (2019), pp. 24–36. DOI: <https://doi.org/10.1016/j.commatsci.2018.07.043>.

[46] Motoko: a data preserving asynchronous orchestrator. <https://gitlab.com/blackdynamite/motoko>.

[47] Autopot: <https://gitlab.com/mhodapp/autopot>.

[48] Konstantin Gubaev, Evgeny V. Podryabinkin, and Alexander V. Shapeev. "Machine learning of molecular properties: Locality and active learning". In: *The Journal of Chemical Physics* 148.24 (June 28, 2018), p. 241727. DOI: [10.1063/1.5005095](https://doi.org/10.1063/1.5005095).

[49] S. A. Goreinov et al. “How to Find a Good Submatrix”. In: Vadim Olshevsky and Eugene Tyrtyshnikov. *Matrix Methods: Theory, Algorithms and Applications*. WORLD SCIENTIFIC, Apr. 2010, pp. 247–256. DOI: [10.1142/9789812836021_0015](https://doi.org/10.1142/9789812836021_0015).

[50] Ivan S Novikov et al. “The MLIP package: moment tensor potentials with MPI and active learning”. In: *Machine Learning: Science and Technology* 2.2 (Jan. 1, 2021), p. 025002. DOI: [10.1088/2632-2153/abc9fe](https://doi.org/10.1088/2632-2153/abc9fe).

[51] M. Hodapp and A. Shapeev. “Machine-learning potentials enable predictive and tractable high-throughput screening of random alloys”. In: *Physical Review Materials* 5.11 (Nov. 22, 2021), p. 113802. DOI: [10.1103/PhysRevMaterials.5.113802](https://doi.org/10.1103/PhysRevMaterials.5.113802).

[52] I. Novikov et al. “AI-accelerated materials informatics method for the discovery of ductile alloys”. In: *Journal of Materials Research* 37.21 (Nov. 14, 2022), pp. 3491–3504. DOI: [10.1557/s43578-022-00783-z](https://doi.org/10.1557/s43578-022-00783-z).

[53] Flyte Contributors. *Flyte: Cloud-Native Workflow Orchestration Platform*. <https://github.com/flyteorg/flyte>. Apache License 2.0, open-source project. 2025.

[54] Kubeflow Community. *Kubeflow Pipelines*. <https://github.com/kubeflow/pipelines>. Apache License 2.0. 2025.

[55] MLflow Contributors. *MLflow*. <https://github.com/mlflow/mlflow>. Apache License 2.0. 2025.

[56] Apache Software Foundation. *Apache Airflow*. <https://github.com/apache/airflow>. Apache License 2.0. 2025.

[57] ZenML Contributors. *ZenML*. <https://github.com/zenml-io/zenml>. Apache License 2.0. 2025.

[58] Netflix and Metaflow Community. *Metaflow*. <https://github.com/Netflix/metaflow>. Apache License 2.0. 2025.

[59] Scikit-learn Developers. *Scikit-learn: Machine Learning in Python*. <https://github.com/scikit-learn/scikit-learn>. BSD 3-Clause License. 2025.

[60] Guillaume Anciaux and the BlackDynamite contributors. *BlackDynamite: A Scientific Parametric-Study Tool*. <https://gitlab.com/ganciaux/blackdynamite>. Version 1.3.3, GPL-3.0-or-later. 2025.

[61] Zope Foundation. *ZODB: A Native Object Database for Python*. <https://www.zodb.org/>. Version 5.x. 2024.

[62] Zope Foundation. *ZEO: Zope Enterprise Objects*. <https://github.com/zopefoundation/ZE0>. Networked Storage Server for ZODB. 2024.

[63] Ask Hjorth Larsen et al. “The atomic simulation environment—a Python library for working with atoms”. In: *Journal of Physics: Condensed Matter* 29.27 (July 12, 2017), p. 273002. DOI: [10.1088/1361-648X/aa680e](https://doi.org/10.1088/1361-648X/aa680e).

[64] G. Kresse and J. Furthmüller. “Efficient iterative schemes for *ab initio* total-energy calculations using a plane-wave basis set”. In: *Physical Review B* 54.16 (Oct. 15, 1996), pp. 11169–11186. DOI: [10.1103/PhysRevB.54.11169](https://doi.org/10.1103/PhysRevB.54.11169).

[65] P. E. Blöchl. “Projector augmented-wave method”. In: *Physical Review B* 50.24 (Dec. 15, 1994), pp. 17953–17979. DOI: [10.1103/PhysRevB.50.17953](https://doi.org/10.1103/PhysRevB.50.17953).

[66] G. Kresse and D. Joubert. “From ultrasoft pseudopotentials to the projector augmented-wave method”. In: *Physical Review B* 59.3 (Jan. 15, 1999), pp. 1758–1775. DOI: [10.1103/PhysRevB.59.1758](https://doi.org/10.1103/PhysRevB.59.1758).

[67] John P. Perdew, Kieron Burke, and Matthias Ernzerhof. “Generalized Gradient Approximation Made Simple”. In: *Physical Review Letters* 77.18 (Oct. 28, 1996), pp. 3865–3868. DOI: [10.1103/PhysRevLett.77.3865](https://doi.org/10.1103/PhysRevLett.77.3865).

[68] L. Mismetti and M. Hodapp. “Automated atomistic simulations of dissociated dislocations with *ab initio* accuracy”. In: *Physical Review B* 109.9 (Mar. 27, 2024), p. 094120. DOI: [10.1103/PhysRevB.109.094120](https://doi.org/10.1103/PhysRevB.109.094120).

[69] J. Byggmästar et al. “Machine-learning interatomic potential for radiation damage and defects in tungsten”. In: *Physical Review B* 100.14 (Oct. 17, 2019), p. 144105. DOI: [10.1103/PhysRevB.100.144105](https://doi.org/10.1103/PhysRevB.100.144105).

[70] ShuoZhi Xu et al. “Frank-Read source operation in six body-centered cubic refractory metals”. In: *Journal of the Mechanics and Physics of Solids* 141 (Aug. 2020), p. 104017. DOI: [10.1016/j.jmps.2020.104017](https://doi.org/10.1016/j.jmps.2020.104017).

[71] V. Vitek. “Theory of the core structures of dislocations in body-centered-cubic metals”. In: *Crystal Lattice Defects* 5 (1974), pp. 1–34.

[72] Xiang-Guo Li et al. “Complex strengthening mechanisms in the NbMoTaW multi-principal element alloy”. In: *npj Computational Materials* 6.1 (June 2, 2020), p. 70. DOI: [10.1038/s41524-020-0339-0](https://doi.org/10.1038/s41524-020-0339-0).

[73] M. Hodapp. “Exact average many-body interatomic interaction model for random alloys”. In: *Computational Materials Today* 5 (Mar. 2025), p. 100018. DOI: [10.1016/j.commt.2024.100018](https://doi.org/10.1016/j.commt.2024.100018).

[74] Tobias Spitaler et al. “Ab-initio grain boundary thermodynamics beyond the dilute limit”. In: *Acta Materialia* 286 (Mar. 2025), p. 120725. DOI: [10.1016/j.actamat.2025.120725](https://doi.org/10.1016/j.actamat.2025.120725).

[75] Yong-Jie Hu et al. “Screening of generalized stacking fault energies, surface energies and intrinsic ductile potency of refractory multicomponent alloys”. In: *Acta Materialia* 210 (May 2021), p. 116800. DOI: [10.1016/j.actamat.2021.116800](https://doi.org/10.1016/j.actamat.2021.116800).

[76] Surya T. Bijualla, Susan R. Atlas, and Pankaj Kumar. *Elastic tensor-derived properties of composition-dependent disordered refractory binary alloys using DFPT*. Nov. 4, 2025. DOI: [10.48550/arXiv.2501.00127](https://doi.org/10.48550/arXiv.2501.00127). arXiv: [2501.00127\[cond-mat\]](https://arxiv.org/abs/2501.00127).

[77] Maksim Kulichenko et al. “Uncertainty-driven dynamics for active learning of interatomic potentials”. In: *Nature Computational Science* 3.3 (Mar. 6, 2023), pp. 230–239. DOI: [10.1038/s43588-023-00406-5](https://doi.org/10.1038/s43588-023-00406-5).

[78] Adam Thomas-Mitchell, Glenn Hawe, and Paul L A Popelier. “Calibration of uncertainty in the active learning of machine learning force fields”. In: *Machine Learning: Science and Technology* 4.4 (Dec. 1, 2023), p. 045034. DOI: [10.1088/2632-2153/ad0ab5](https://doi.org/10.1088/2632-2153/ad0ab5).

[79] Cheuk Hin Ho, Christoph Ortner, and Yangshuai Wang. *Flexible Uncertainty Calibration for Machine-Learned Interatomic Potentials*. Oct. 1, 2025. DOI: [10.48550/arXiv.2510.00721](https://doi.org/10.48550/arXiv.2510.00721). arXiv: [2510.00721\[physics\]](https://arxiv.org/abs/2510.00721[physics]).

[80] Yifeng Tian et al. “Data-driven modeling of dislocation mobility from atomistics using physics-informed machine learning”. In: *npj Computational Materials* 10.1 (Sept. 14, 2024), p. 219. DOI: [10.1038/s41524-024-01394-4](https://doi.org/10.1038/s41524-024-01394-4).

[81] Petr Grigorev et al. “matscipy: materials science at the atomic scale withPython”. In: *Journal of Open Source Software* 9.93 (Jan. 28, 2024), p. 5668. DOI: [10.21105/joss.05668](https://doi.org/10.21105/joss.05668).

[82] Erik Bitzek et al. “Structural Relaxation Made Simple”. In: *Physical Review Letters* 97.17 (Oct. 27, 2006), p. 170201. DOI: [10.1103/PhysRevLett.97.170201](https://doi.org/10.1103/PhysRevLett.97.170201).

[83] Graeme Henkelman and Hannes Jónsson. “Improved tangent estimate in the nudged elastic band method for finding minimum energy paths and saddle points”. In: *The Journal of Chemical Physics* 113.22 (Dec. 8, 2000), pp. 9978–9985. DOI: [10.1063/1.1323224](https://doi.org/10.1063/1.1323224).